Received: 26 August 2021 | Revised: 7 September 2021 | Accepted: 12 September 2021

DOI: 10.1002/pol.20210664

RESEARCH ARTICLE

JOURNAL OF POLYMER SCIENCE WILEY

Polyamide membranes enabled by covalent organic framework nanofibers for efficient reverse osmosis

Guanghui Yang | Zhe Zhang | Congcong Yin | Xiansong Shi | Yong Wang

State Key Laboratory of Materials-Oriented Chemical Engineering, College of Chemical Engineering, Nanjing Tech University, Nanjing, P. R. China

Correspondence
Zhe Zhang and Yong Wang, State Key Laboratory of Materials-Oriented Chemical Engineering, College of Chemical Engineering, Nanjing Tech University, Nanjing 211816, P. R. China.
Email: zhangzhe@njtech.edu.cn (Z. Z.) and yongwang@njtech.edu.cn (Y. W.)

Funding information
National Natural Science Foundation of China, Grant/Award Number: 21825803

Abstract

Polyamide reverse osmosis membranes are indispensable for the worldwide clean water supply. Incorporation of nanomaterials into polyamide separation layer provides an evident methodology to enhance the water flux. However, the desalination performance would be compromised by the inadequate compatibility between the nanomaterial and the polyamide matrix. In this work, we propose a straightforward strategy to use covalent organic frameworks (COF) nanofibers as the efficient nanofiller for the fabrication of high flux polyamide membranes. The COF nanofibers featuring crystalline structures, large surface area and well-defined micropores are synthesized by a surfactant-mediated solvothermal method. It is found that the COF nanofibers are able to mediate the interfacial polymerization process via the controlled release of amine molecules. This creates the reduced thickness of the polyamide separation layer. Moreover, the rigid and permanent nanopores of COF could serve as additional channels for water permeation. Benefitting from the low thickness and the additional channels, thus fabricated membranes exhibit a significantly enhanced water flux, while maintaining a slightly improved NaCl rejection. Our work is expected to provide a new insight for the design and fabrication of advanced polyamide reverse osmosis membranes.

KEYWORDS

covalent organic frameworks, desalination, nanofibers, reverse osmosis, thin-film nanocomposite membrane

1 | INTRODUCTION

Reverse osmosis (RO) has been widely recognized as an indispensable membrane-based separation technology for brackish water and seawater desalination, which is ubiquitous in worldwide clean water supply, owing to the advantages of high separation efficiency, operational flexibility, small footprints.[1–3] State-of-the-art RO membranes possess a thin-film composite (TFC) configuration, which are composed of a fully aromatic polyamide separation layer and a tightly attached porous polysulfone (PSF) substrate.[4,5] Polyamide films (separation layers) are created by the polycondension between two multifunctional monomers, such as trimesoyl chloride (TMC) and *m*-phenylenediamine (MPD).[6,7] These monomers are individually dissolved in organic and aqueous solutions to provide a stable interface by two immiscible phases so that the insoluble polymeric film can be formed.[8,9] Because the chlorine atoms in acid chlorides are electron-withdrawing groups, which endow the carbon atoms with enhanced electrophilicity, making acid chlorides more susceptible to the nucleophilic attacking of amines.[10] Thus, the reaction between TMC and MPD is extremely fast and irreversible that leads to the formation of highly cross-linked polymer networks.

Besides, the relatively uncontrollable reaction inevitably results in a local temperature rise at the interface.[11,12] Consequently, the rapid dissipation of heat toward the organic solutions generates the leaf-like, crumpled separation layer.[13,14] The crumpled layers typically have a ridge-and-valley structure, and the distance between the ridge and valley is widely considered as the thickness (apparent thickness) of the separation layer, which is usually reported to be ~50–200 nm.[15] However, conventional polyamide RO membranes suffer from the relatively low water permeation rate (water flux), due to the high transport resistance derived from the highly cross-linked polyamide layers with large thicknesses and crumpled structures.

The introduction of nanomaterials into the polyamide separation layer to fabricate thin-film nanocomposite (TFN) membranes is thought to be a straightforward strategy to elevate the water flux while maintaining a satisfying salt rejection rate.[16,17] Nanomaterials are mainly used as the nanofiller (dispersed phase) to dope into the polyamide matrix, on account of their diverse functionalities such as inherent porous, charge properties and surface functional groups. For nonporous nanomaterials, such as SiO_2,[18,19] carbon nanotubes (CNTs),[20,21] and MXenes,[22] it is proved that the water flux can be enhanced by the presence of interfacial voids between the nanofiller and the matrix. For porous nanomaterials such as metal–organic frameworks (MOFs)[23] and zeolites,[24] in addition to the interfacial voids, a large number of interior pores are also able to provide channels for water permeation. In this scenario, therefore, porous nanofillers would lead to much pronounced flux enhancement. For instance, Hoek and coworkers have demonstrated that porous zeolite can create preferential channels in polyamide separation layer for water permeation.[24] The resultant membrane exhibited significant enhancement of water flux without compromising salt rejection rate. Given the above, the inherent pore of nanofiller along with the molecular-scale voids between the nanofiller and polyamide matrix can both function as additional water transport channels.[25,26] Nonetheless, many of those nanomaterials are composed of an inorganic or inorganic–organic component, and usually do not have a favorable compatibility between the nanofiller and the matrix, resulting in non-selective interface defects.[16,22] As a consequence, these defects would compromise the salt rejection rate to some extent. Thus, new materials with better compatibility should be sought to tackle this challenge.

Covalent organic frameworks (COFs) are crystalline framework materials, which are formed via reticulation process, in which the pure organic building blocks are bonded into extended structures with strict periodicity and distinct regularity.[27,28] COFs have the advantages of well-defined nanoporosity, low density, good chemical stability and facilely tailored functionalities.[29,30] Especially, when working as the nanofiller, the rigid nanopores as well as the entirely organic backbones are eligible for the fabrication of polyamide TFN membranes.[31,32] The rigid nanopores provide permanent channels for water permeation, and organic nature enables excellent compatibility. For instance, in previous work, we deposited cationic COF nanofibers on macroporous substrates to form scaffolds for the construction of polyamide separation layers with ultrathin thicknesses and enlarged permeation areas.[33] Benefitting from the mediation effect of nanofiber scaffolds as well as the excellent compatibility between COF and polyamide, the resultant membranes exhibited an exceptional nanofiltration performance. Herein, we proposed an evident strategy to use a β-ketoenamine-linked COF, TpPa, as the nanofiller for the fabrication of TFN membranes with upgraded microstructures and enhanced water flux. The fibrous TpPa, which was created by the surfactant-mediated solvothermal synthesis, was used as the nanofiller for the fabrication of TFN membranes via interfacial polymerization (Scheme 1). TpPa nanofibers with crystalline structure and high porosity worked as a mediator to effectively adsorb and controllably release MPD molecules, capable of controlling the interfacial polymerization process. Thus, the thinner thickness of the separation layer can be formed. Besides, the rigid and permanent nanopores of TpPa nanofibers would also function as the additional water permeation channels. Benefitting from the reduced thickness as well as the created permeation channels, thus fabricated TFN membranes exhibited an up to ~2-fold enhancement of water flux, alongside a slightly improved NaCl rejection, compared to the control membrane. This work demonstrated that TpPa nanofibers with an excellent compatibility to polyamide matrix can be used as the nanofillers to prepare high-flux RO membranes. This is distinguished from the strategy of the construction of COF scaffolds in our previous work.[33]

2 | EXPERIMENTAL SECTION

2.1 | Materials

1,3,5-Triformylphloroglucinol (Tp) was supplied by Jilin Chinese Academy of Sciences-Yanshen Technology Co., Ltd. *p*-Phenylenediamine (Pa), hexadecyltrimethylammonium bromide (CTAB, 99%), sodium dodecyl sulfate (SDS, 98.5%), MPD, and TMC were purchased from Shanghai Aladdin Biochemical Technology Co., Ltd. Polysulfone (PSF) ultrafiltration membranes (molecular weight cut-off, 20,000 Da) were obtained from RisingSun Membrane Technology Co., Ltd. Other chemical reagents were commercially available. Unless elsewhere indicated, all reagents were used without

SCHEME 1 Schematic diagram of the fabrication of TFN membranes

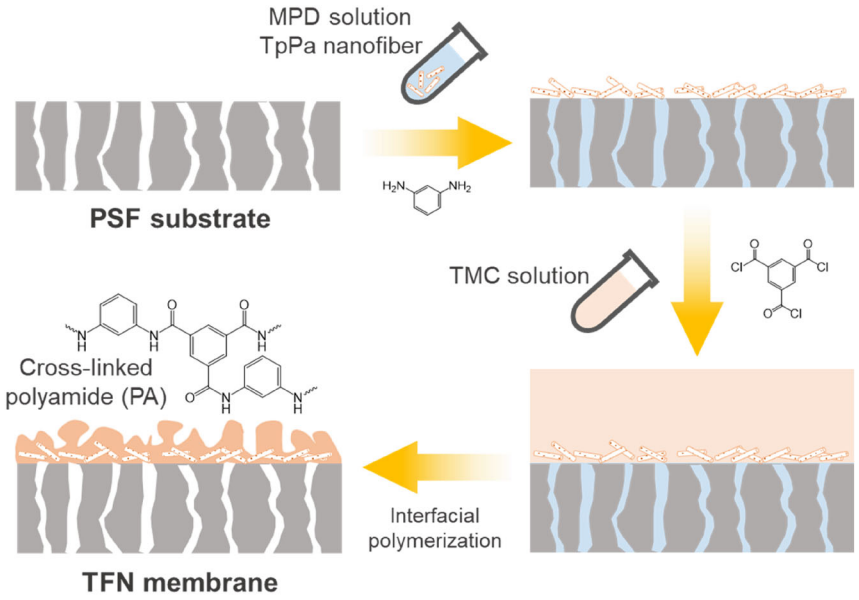

further purification. Deionized water (DI water, conductivity <10 μS cm^{-1}) was used throughout all experiments.

2.2 | Synthesis of TpPa nanofibers

TpPa nanofibers were synthesized by the surfactant-mediated solvothermal method. First, Tp and Pa solutions were prepared, respectively. Briefly, Tp or Pa was dissolved in 1,4-dioxane (250 μL) and then added to CTAB aqueous solution (0.1 mol L^{-1}, 45 mL) followed by sonication treatment. Then the SDS aqueous solution (0.1 mol L^{-1}, 3.4 mL) was added. The two monomer solutions were mixed and charged into round-bottom glass tubes. Next, 10 mL of acetic acid was added. The tubes were frozen in liquid nitrogen, degassed by three freeze-pump-thaw cycles, and sealed under vacuum. The tubes were heated at 30°C for 72 h. The reddish-brown precipitates were obtained by ammonia water neutralization (10 mL) and ethanol demulsification (100 mL). The precipitates were further filtered, thoroughly washed with ethanol and water, and vacuum-dried at 70°C for 24 h. Note that, the isolated powders were used for the characterizations, while the TpPa solutions after reaction were directly used for the fabrication of membranes.

2.3 | Fabrication of RO membranes

The aqueous dispersions of TpPa nanofibers were prepared by directly diluting the solutions after reaction using water, followed by sonication treatment for 30 min. To prepare the amine solutions for interfacial polymerization, MPD (2%, w/v) was added into the TpPa aqueous dispersions. The concentrations of TpPa nanofibers in amine solutions were 1, 2, 3, and 5 mg L^{-1}, respectively.

The membranes were prepared by interfacial polymerization using PSF ultrafiltration membrane as the substrate. In a typical process, the substrate was horizontally fixed into a custom-built device, in which the edge of the substrate was sealed with O-ring and a stainless-steel frame. Next, 30 mL of amine solutions were poured onto the device to contact the upper surface of PSF substrate, which is maintained for 60 s. The amine solution was drained, and the PSF substrate was taken out from the device. A rubber roller was then used to remove the surface-adhered aqueous solution. Next, the PSF substrate impregnated with amine solution was replaced into the device, and 10 mL of organic solution (TMC dissolved in *n*-hexane, 0.2%, w/v) was poured into the device, standing for 60 s, to accomplish the interfacial polymerization. After the reaction, organic solution was dumped, and the membrane was cured at 60°C for 10 min. The membranes were stored in water for further use. The TpPa incorporated membrane with TpPa concentration of 2 mg L^{-1} was named as PA-COF. For comparison, control membrane (named as PA) was prepared by the same method except for the addition of TpPa nanofibers.

2.4 | Characterizations

The chemical structures of TpPa and membranes were revealed by Fourier transform infrared spectroscopy (FTIR, Nicolet 8700, Thermo Fisher Scientific). The membrane samples were analyzed under an attenuated total reflectance mode (ATR). The elemental compositions of membranes were evaluated by X-ray photoelectron spectroscopy

(XPS, AXIS Ultra DLD, Shimadzu). The crosslinking degree of membranes was calculated based on the atomic ratio of oxygen over nitrogen (O/N) as following:

$$r = \frac{O}{N} = \frac{(3x+4y)}{(3x+2y)} \quad (1)$$

$$n = \frac{x}{x+y} = \frac{(4-2r)}{(1+r)} \quad (2)$$

where x and y represent the cross-linked and linear parts in the polyamide layer, respectively. r is the ratio of the atomic ratio of oxygen over nitrogen (O/N) and n is the crosslinking degree of membranes.[34,35] Scanning electron microscopy (SEM) images of TpPa and membranes were captured on a field-emission electron microscope (S-4800, Hitachi) operating at 3 kV. The samples were sputter-coated with a layer of gold on a MC1000 ion-sputtering apparatus before imaging. High-resolution transmission electron microscopy (HRTEM) images of TpPa were obtained using a JEM-2100 microscope (JEOL) operating at 200 kV. Samples were prepared by drop-casting TpPa aqueous dispersion over a copper grid. Nitrogen adsorption–desorption isotherms of TpPa were measured on a surface area and porosimetry system (ASAP2460, Micromeritics). Brunauer–Emmett–Teller (BET) analysis was used to evaluate the surface areas. The pore width distribution was acquired by nonlocal density functional theory (NLDFT) model. The surface topography of membranes was obtained by atomic force microscopy (AFM, XE-100, Park Systems) imaging. The contact angle membranes were determined on a goniometer (Drop Meter A100P, MAIST). The surface charge properties of membranes were recorded on an electrokinetic analyzer (SurPASS, Anton Paar GmbH) using a streaming potential method. KCl aqueous solution (0.1 mmol L^{-1}) was chosen as the background solution. The pH values throughout the test were adjusted by 0.1 mol L^{-1} NaOH and HCl solutions, respectively.

2.5 | RO performance evaluation

The RO performances including water flux and NaCl rejection were evaluated on a bench-scale cross-flow filtration setup. The effective membrane area was 28.3 cm^2. The testing pressure was fixed at 1 MPa, and the volume flow rate was maintained at 35 L h^{-1}. The temperature of the testing solution was controlled at 25°C. All membranes were pressurized at 1 MPa for 1 h to reach a steady permeation flux prior to testing. The concentration of NaCl aqueous solution was 2000 ppm. The water flux (J_w, L m^{-2} h^{-1}) and NaCl rejection rate (R, %) were calculated as following:

$$J_w = \frac{\Delta V}{A \times \Delta t} \quad (3)$$

$$R = \left(1 - \frac{C_p}{C_f}\right) \times 100\% \quad (4)$$

where ΔV (L) is the volume of the filtrate, A (m^2) is the effective membrane area, Δt (h) is the filtration time. C_p and C_f are the concentrations of the filtrate and the feed solution, respectively. The concentration of NaCl aqueous solution was calculated by a conductivity meter (S230-K, Mettler-Toledo).

3 | RESULTS AND DISCUSSION

3.1 | Synthesis and characterization of TpPa nanofibers

In this article, TpPa was synthesized by a Schiff-base condensation reaction between Pa and Tp (Figure 1(A)). The chemical structures of TpPa were confirmed by the FTIR spectrum (Figure 1(B)), as two characteristic peaks of C=C bond (1580 cm^{-1}) and C—N bond (1256 cm^{-1}) appeared. This indicates the formation of the β-ketoenamine linkage, evidencing the successful synthesis of TpPa.[36,37] We further observed the morphology of TpPa by SEM imaging (Figure 1(C)). TpPa exhibits fiber-like morphology with a diameter of ~20 nm, and a length of up to hundreds of nanometers. During the synthesis of TpPa nanofibers, surfactants were used to mediate the formation of fiber-like morphology. The surfactants can encapsulate the monomers and prepolymers to form micelles,[38] which is beneficial to form well-defined nanostructures, rather than irregularly shaped bulks. Meanwhile, excess acetic acid (10 mL) is able to protonate the amino groups of the prepolymers, thus slowing their ripening processes. Therefore, under the synergistic enhancement of surfactant mediation and acid adjustment, TpPa with fiber-like morphology was created. Besides, TpPa nanofibers can be well dispersed in water and stand for 3 months without any precipitation (Figure S1), due to the amphiphilic nature of surfactants. The crystalline characteristic of TpPa nanofibers was further investigated by HRTEM (Figure 1(D)). Interestingly, we obtained a single fiber, the diameter of which is well matched with that of the SEM observation. The lattice fringes can be clearly seen in HRTEM and inverse fast Fourier transform (IFFT) images, evidencing the crystalline nature of TpPa nanofiber. The porosity of TpPa nanofibers was studied by the nitrogen adsorption–desorption test. As

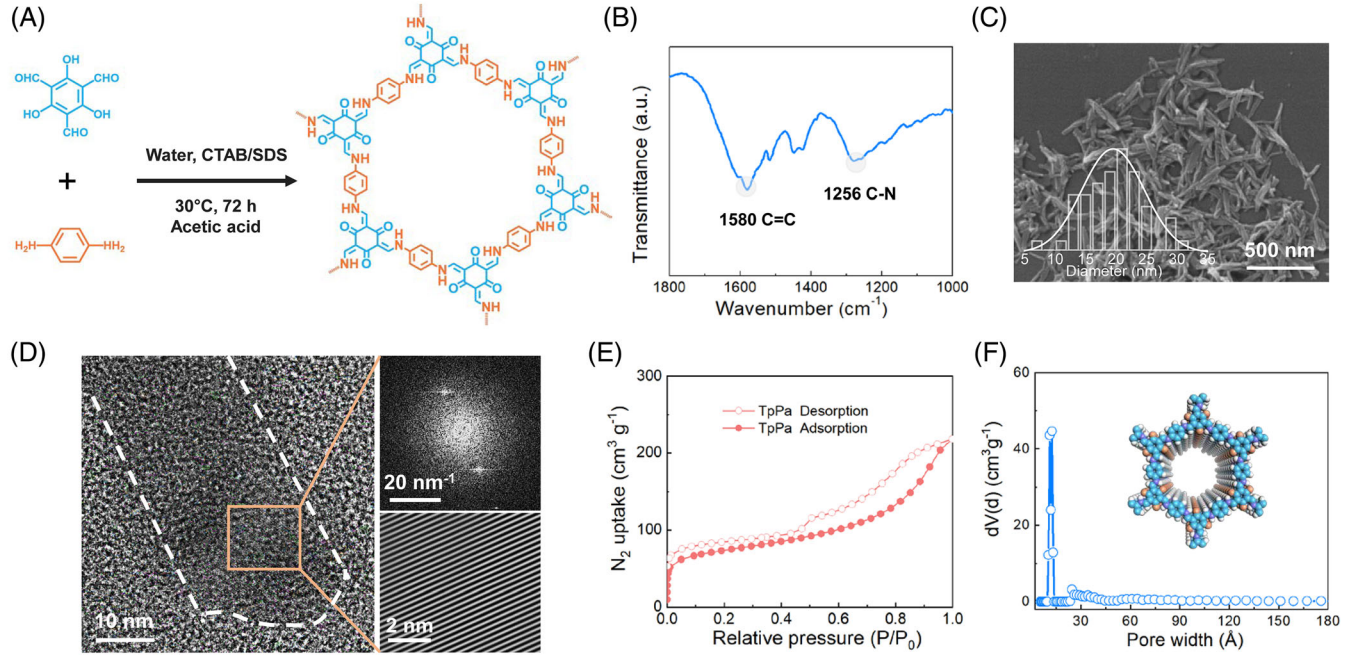

FIGURE 1 Characterization of TpPa nanofibers. (A) Synthetic scheme of TpPa. (B) FTIR spectrum of TpPa. (C) SEM image of TpPa nanofiber (inset shows the diameter distribution of TpPa nanofibers). (D) HRTEM image of TpPa nanofiber along with fast Fourier transform (FFT) (top-right) and inverse fast Fourier transform (IFFT) images (bottom-right). (E) Nitrogen adsorption–desorption isotherm of TpPa nanofibers. (F) Pore width distribution of TpPa nanofibers (inset shows the structural model of TpPa nanofibers)

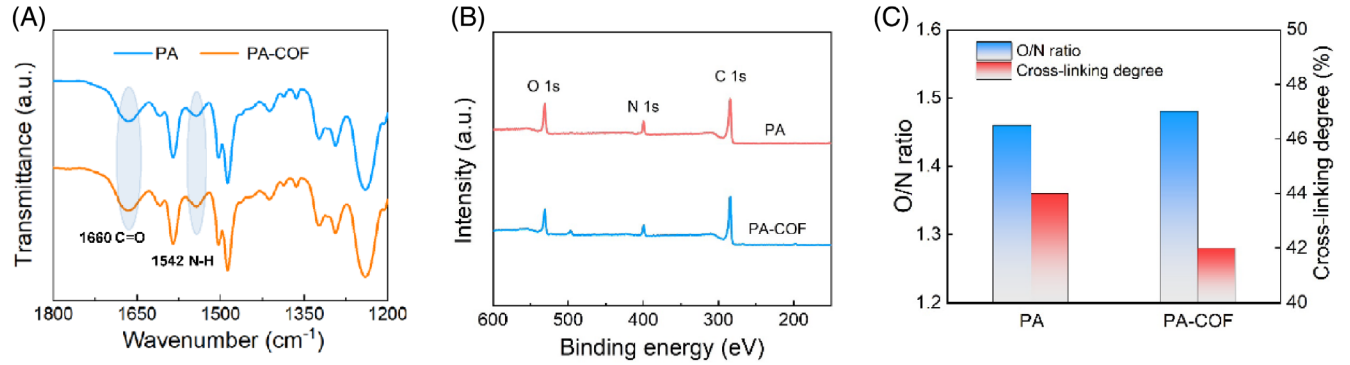

FIGURE 2 Chemical properties of PA and PA-COF membranes. (A) ATR-FTIR spectra, (B) XPS spectra and (C) O/N ratios and cross-linking degrees

shown in Figure 1(E), the BET area of TpPa nanofibers was calculated to be 237.5 $m^2\ g^{-1}$. The pore width of TpPa nanofibers was calculated to be ~1.2 nm based on the NLDFT model (Figure 1(F)). These results indicate that TpPa nanofibers have a favorable microporous structure. On the basis of above, TpPa nanofibers with high crystallinity and porosity were successfully synthesized.

3.2 | Characterization of membranes

The TFN membranes were fabricated by the interfacial polymerization using PSF as the substrate. The chemical structure of the separation layer was analyzed by ATR-FTIR spectra. As shown in Figure 2(A), the appearance of C=O stretching vibration peak at 1660 cm^{-1} and N—H bending vibration peak at 1542 cm^{-1} verify the formation of polyamide network.[39] Notable that, the characteristic peaks of TpPa were not detected in these spectra, probably because the incorporation amount of TpPa nanofibers inside polyamide layer was relatively low. We further adopted XPS to reveal the chemical composition of the membranes. The elements of C, N, O were detected in both PA and PA-COF membranes (Figure 2(B)), indicative of the similar chemical composition. To gain further structural properties, the O/N ratio and cross-linking

degree were used to describe the properties of polyamide networks (Figure 2(C)). After the incorporation of TpPa nanofibers, the O/N ratio increased from 1.46 to 1.48, while the cross-linking degree slightly decreased from 44% to 42%. This results can be attributed as following: Since the edge of TpPa nanofibers possess a number of unreacted amino groups, they would further react with the TMC during the interfacial polymerization. This reduces the cross-linking degree. Moreover, the amount of oxygen is slightly higher than that of nitrogen in the backbone of TpPa, which increases the O/N ratio.

To probe the effects of the incorporation of TpPa nanofibers on the surface properties of the separation layers, the measurements of the water contact angle and Zeta potential of the membranes were conducted, respectively. As shown in Figure 3(A), with the incorporation of TpPa nanofibers, the water contact angles of membranes decreased from 78° to 60°. The decline of water contact angle is probably related to the change of surface roughness according to the Wenzel equation[40,41]:

$$\cos\theta_2 = r \times \cos\theta_1 \tag{5}$$

where θ_1 and θ_2 are the contact angles of the actual surface and projection surface, respectively, and r is the roughness factor, which is defined as the ratio of the actual surface area to the projection area. The Wenzel equation describes that when the contact angle is lower than 90°, the contact angle would decrease with the increase of surface roughness. In this case, the incorporation of TpPa nanofibers would enhance the surface roughness, which will be discussed later. This leads to the reduced water contact angle, that is, the enhanced surface hydrophilicity, which is favorable to the water flux enhancement. As shown in Figure 3(B), with the incorporation of TpPa nanofibers, Zeta potentials of membranes increased from ~30 mV to ~20 mV under a neutral pH environment. The polyamide networks are formed by the fast and irreversible reaction between TMC and MPD, a number of acyl chloride groups of TMC could not effectively react with MPD to form the network. Thus, the residual acyl chloride groups would hydrolyze into carboxyl groups, rendering the negatively charged polyamide layers.[42] As we referred above, nevertheless, the edge of TpPa nanofibers possess unreacted amino groups, and they would also react with the TMC, preventing the acyl chloride groups from hydrolysis. Thereby, the negative charge of the PA-COF membrane is weakened.

In order to understand the effects of the incorporation of TpPa nanofibers on the variation of the surface morphology of the separation layers, SEM imaging of the membrane was carried out (Figure 4). The PSF substrate exhibits a smooth and porous surface morphology (Figure S2). After the interfacial polymerization, all membranes possess a rough and crumpled separation layer (Figure 4(A)–(F)). The surface morphology exhibits a leaf-like and ridge-and-valley structure, which is thought to be the representative feature of the polyamide film prepared by interfacial polymerization of MPD and TMC.[14] For PA membrane, the large leaf-like structures can be clearly seen on its surface (Figure 4(A) and (B)). The thickness of separation layer of PA membrane is measured to be ~206 nm (Figure 4(C)). When TpPa nanofibers were incorporated into the polyamide separation layer, the leaf-like structure on the surface became smaller (Figure 4(D) and (E)). The thickness of the separation layer reduced to ~157 nm (Figure 4(F)).

We further investigated the TpPa concentration of the amine solutions on the morphology evolutions of separation layers. When the concentration of TpPa nanofibers was 1 mg L^{-1}, the surface of the separation layer exhibited a similar morphology with the large leaf-like structure compared to that of PA membrane (Figure 5(A)). The thickness of the separation layer was slightly reduced to ~196 nm (Figure 5(D)). With the TpPa concentration further increased to 3 mg L^{-1}, some leaf-like structures were prone to fuse together, forming larger structures (Figure 5(B)). Thickness of the separation layer increased to ~235 nm (Figure 5(E)). As the TpPa concentration

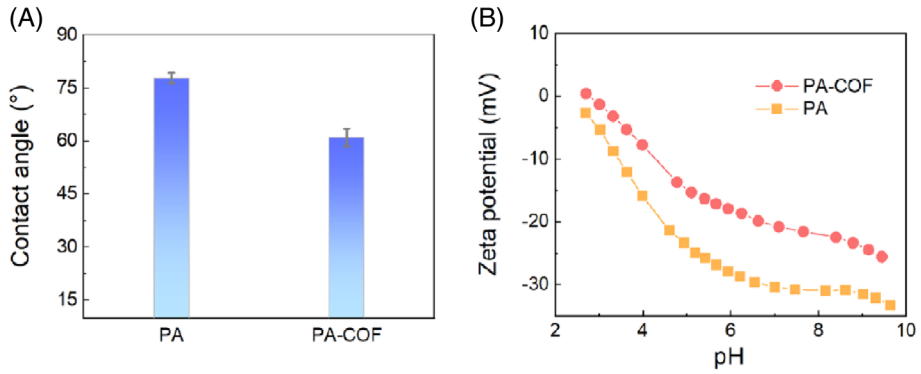

FIGURE 3 Surface properties of PA and PA-COF membranes. (A) Contact angles and (B) Zeta potentials

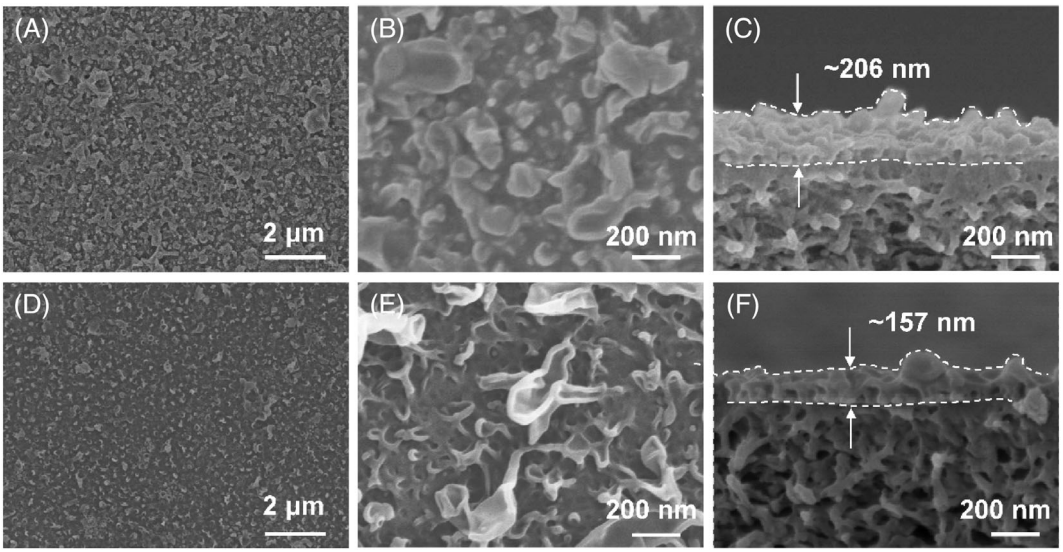

FIGURE 4 SEM characterization of membranes. SEM images of PA membranes: (A) surface at low magnification, (B) surface at high magnification and (C) cross section. SEM images of PA-COF membranes: (D) surface at low magnification, (E) surface at high magnification and (F) cross section

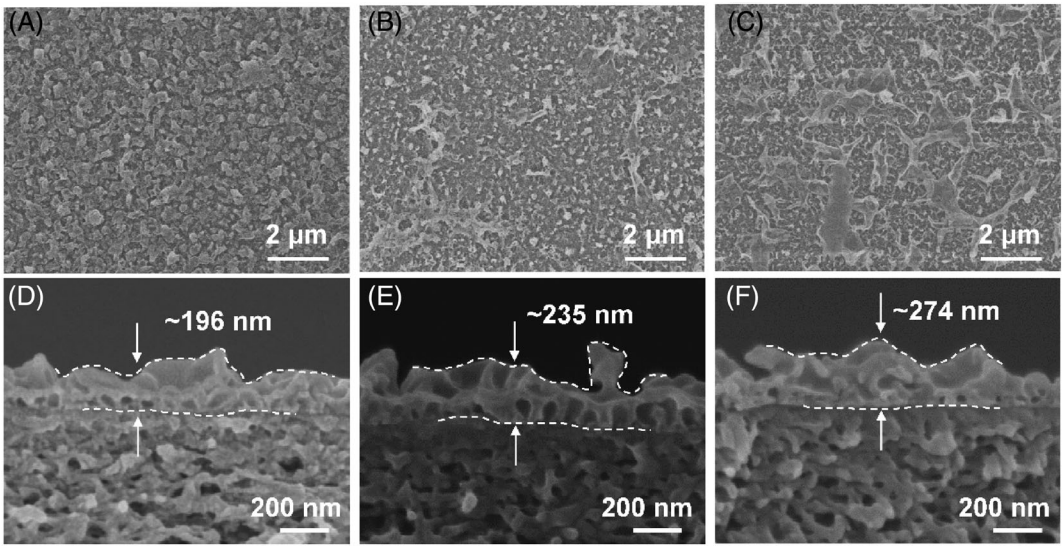

FIGURE 5 SEM characterization of membranes. SEM images of the surface and cross section of PA-COF membranes fabricated from different TpPa concentration: (A, D) 1 mg L^{-1}, (B, E) 3 mg L^{-1}, (C, F) 5 mg L^{-1}

ultimately increased to 5 mg L^{-1}, much larger leaf-like structures appeared (Figure 5(C)). The thickness of the separation layer increased to ~274 nm (Figure 5(F)). These phenomena indicate that the incorporation of TpPa nanofibers would influence the process of interfacial polymerization, and thereby vary the morphology of the separation layer. It is widely accepted that the leaf-like structure of polyamide separation layer is created by the rapid dissipation of heat during the interfacial polymerization.[11–14] During the interfacial polymerization, TpPa nanofibers with large surface area and well-defined micropores can effectively adsorb MPD solution. This would slow the diffusion of MPD toward the organic solution to react with TMC.[43,44] Therefore, after the incorporation of TpPa nanofibers, the fast interfacial reaction can be controlled to some extent. The relatively controlled interfacial polymerization trends to generate thinner polyamide separation layer.[45,46] Thus, low thicknesses of polyamide layer can be formed under the TpPa concentration of 1 and 2 mg L^{-1}. However, large

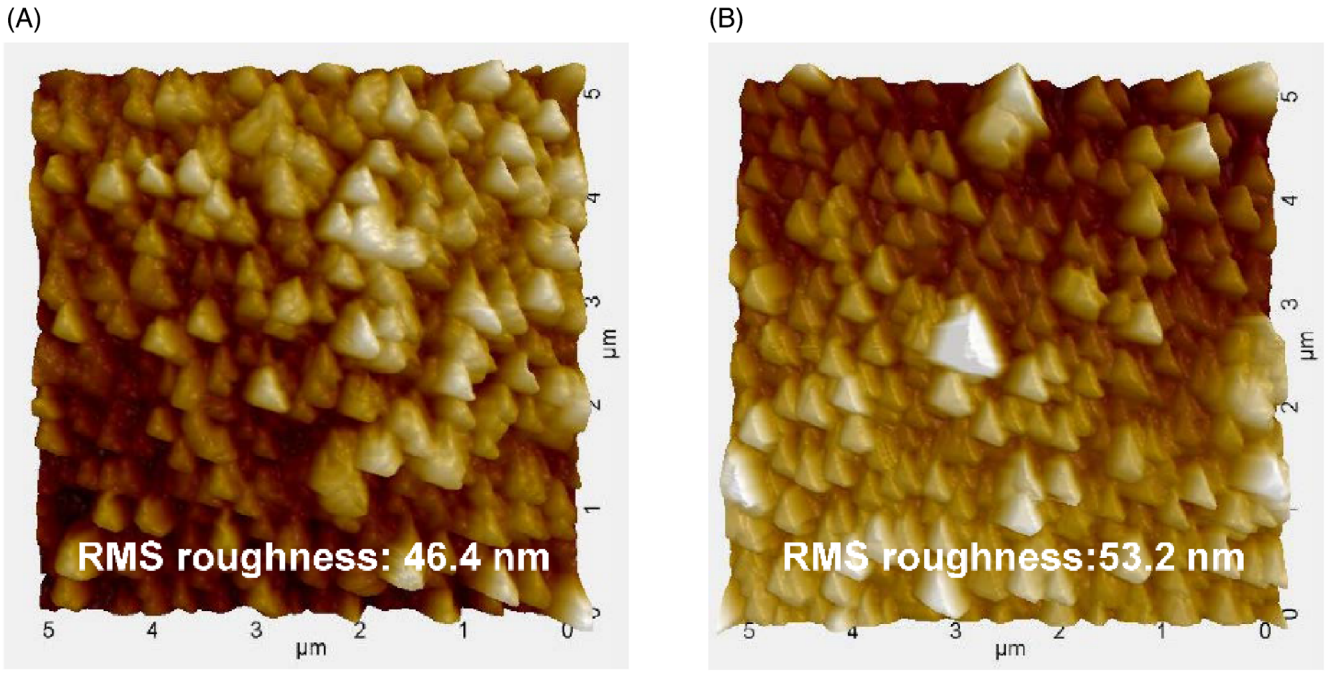

FIGURE 6 AFM topography images of (A) PA membrane and (B) PA-COF membrane (scanning area was 5 μm × 5 μm)

thicknesses of polyamide layer were obtained under the TpPa concentration of 3 and 5 mg L^{-1}. The large amount of TpPa nanofibers would adsorb more MPD solution in their nanopores, making the fast interfacial reaction more controllable. Therefore, the initially formed polyamide layer was very thin, and loosely structured, thus the MPD monomers could further penetrate through such film to continuously react with TMC, forming the polyamide network.[47] As a result, those separation layers possess much larger thicknesses.

Besides, the root mean square (RMS) roughnesses of the separation layers were obtained by AFM testing. As shown in Figure 6, the PA membrane has a RMS roughness of 46.4 nm, while the PA-COF membrane has a RMS roughness of 53.2 nm. As we indicated above, TpPa nanofibers can mediate the interfacial polymerization process, capable of varying the morphology of the separation layer. The leaf-like structure became smaller after the mediation of TpPa nanofibers. Thus, the RMS roughness of PA-COF is slightly increased. This result also provides direct evidence for the decline of water contact angle, which has been mentioned previously.

3.3 | RO performance of membranes

To reveal the structure-performance relationship, we investigated the RO performance of membranes fabricated under various TpPa concentrations. As shown in Figure 7, without the incorporation of TpPa nanofibers,

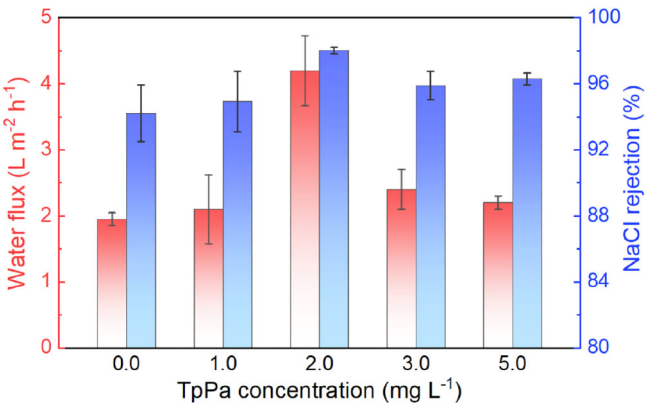

FIGURE 7 RO performances of different membranes

the membrane (PA membrane) exhibited a low water flux of 1.9 L m^{-2} h^{-1}, and a NaCl rejection rate of 94.2%. When TpPa concentration was 1 mg L^{-1}, the membrane demonstrated a slightly increased water flux and NaCl rejection rate. However, as the TpPa concentration increased to 2 mg L^{-1}, the membrane has an optimal RO performance with a water flux of 4.2 L m^{-2} h^{-1}, and a NaCl rejection rate of 98.0%. With the TpPa concentration further increased to 3 and 5 mg L^{-1}, the water flux and NaCl rejection rate were both reduced. Based on the above results, the enhancement of water flux can be ascribed to the reduced thickness of separation layers as well as the additional water channels provided by the TpPa nanofibers. Without the incorporation of TpPa nanofibers, the interfacial polymerization is relatively

uncontrollable, which results in thick separation layer. Thus, PA membrane exhibited a low water flux. With a low concentration of TpPa nanofibers was adopted (1 mg L^{-1}), the mediation of interfacial polymerization was not very significant. Thus, the thickness of the separation layer was slightly reduced, and the membrane did not show an obvious enhancement of water flux. However, under the optimal condition (2 mg L^{-1}), a significant mediation of interfacial polymerization occurred, leading to largely reduced thickness of the separation layer. Hence, the water flux of the membrane can be greatly enhanced. When the concentration of TpPa nanofibers further increased, the mediation of interfacial polymerization became much pronounced, leading to thicker separation layers as we have mentioned above. Those membranes exhibited declined water fluxes. It should be notable that, after the incorporation of TpPa nanofibers, the NaCl rejection of membranes were obviously improved , due to the enhanced compatibility between TpPa nanofibers and the polyamide matrix, as we have discussed previously. Furthermore, the incorporated TpPa nanofibers with large surface area and well-defined micropores could also function as the additional channels for water permeation. The integrity of the nanochannels would not be compromised thanks to the rigid and crystalline structures of TpPa, which is beneficial to the enhancement of water flux.

4 | CONCLUSION

In summary, we demonstrated a straightforward strategy that used TpPa nanofibers as the nanofiller to fabricate TFN membranes. TpPa nanofibers were synthesized via the surfactant-mediated solvothermal synthesis. The synthesized TpPa nanofibers are crystalline and highly porous. TpPa nanofibers worked as the mediator for the controllable formation of polyamide separation layer with significantly reduced thickness via the controlled release of MPD molecules. Furthermore, the rigid and permanent nanopores of TpPa nanofibers functioned as additional channels for water permeation. Benefitting from the reduced thickness as well as the generated water channels, TFN membranes demonstrated an up to ~2-fold enhancement of water flux, while maintaining a satisfying NaCl rejection rate of 98.0%, compared to the control membrane. This work opens up an avenue for the rational design and fabrication of high flux TFN membranes for high-efficient RO.

ACKNOWLEDGMENTS

This work was funded by the National Natural Science Foundation of China (21825803).

DATA AVAILABILITY STATEMENT

The data used to support the findings of this study are available from the corresponding author upon reasonable request.

ORCID

Yong Wang https://orcid.org/0000-0002-8653-514X

REFERENCES

[1] N. A. Ahmad, P. S. Goh, L. T. Yogarathinam, A. K. Zulhairun, A. F. Ismail, *Desalination* **2020**, *493*, 114643.
[2] S. Lin, H. Zhao, L. Zhu, T. He, S. Chen, C. Gao, L. Zhang, *Desalination* **2021**, *498*, 114728.
[3] Y. Yao, P. Zhang, C. Jiang, R. M. DuChanois, X. Zhang, M. Elimelech, *Nat. Sustain.* **2020**, *4*, 138.
[4] Z. Yang, H. Guo, C. Y. Tang, *J. Membr. Sci.* **2019**, *590*, 117297.
[5] M. R. Chowdhury, J. Steffes, B. D. Huey, J. R. McCutcheon, *Science* **2018**, *361*, 682.
[6] S. Habib, S. T. Weinman, *Desalination* **2021**, *502*, 114939.
[7] C. Liu, W. Wang, B. Yang, K. Xiao, H. Zhao, *Water Res.* **2021**, *195*, 116976.
[8] L. E. Peng, Y. Jiang, L. Wen, H. Guo, Z. Yang, C. Y. Tang, *J. Membr. Sci.* **2021**, *625*, 119173.
[9] A. K. Ghosh, B. H. Jeong, X. Huang, E. M. V. Hoek, *J. Membr. Sci.* **2008**, *311*, 34.
[10] D. H. N. Perera, Q. Song, H. Qiblawey, E. Sivaniah, *J. Membr. Sci.* **2015**, *487*, 74.
[11] S. Karan, Z. Jiang, A. G. Livingston, *Science* **2015**, *348*, 1347.
[12] S. J. Vanhook, M. F. Schatz, J. B. Swift, W. D. M. Cormick, H. L. Swinney, *J. Fluid Mech.* **1997**, *345*, 45.
[13] E. M. V. Hoek, S. Bhattacharjee, M. Elimelech, *Langmuir* **2003**, *19*, 4836.
[14] Y. J. Lim, J. Lee, T. H. Bae, J. Torres, R. Wang, *J. Membr. Sci.* **2020**, *611*, 118407.
[15] Z. Jiang, S. Karan, A. G. Livingston, *Adv. Mater.* **2018**, *30*, 1705973.
[16] Z. C. Ng, W. J. Lau, T. Matsuura, A. F. Ismail, *Chem. Eng. Res. Des.* **2021**, *165*, 81.
[17] Z. Yang, H. Guo, Z. K. Yao, Y. Mei, C. Y. Tang, *Environ. Sci. Technol.* **2019**, *53*, 5301.
[18] M. Bao, G. Zhu, L. Wang, M. Wang, C. Gao, *Desalination* **2013**, *309*, 261.
[19] B. T. H. Wu, P. Wu, *J. Membr. Sci.* **2013**, *428*, 341.
[20] H. J. Kim, M. Y. Lim, K. H. Jung, D. G. Kim, J. C. Lee, *J. Mater. Chem. A* **2015**, *3*, 6798.
[21] H. D. Lee, H. W. Kim, Y. H. Cho, H. B. Park, *Small* **2014**, *10*, 2653.
[22] D. L. Zhao, S. Japip, Y. Zhang, M. Weber, C. Maletzko, T. S. Chung, *Water Res.* **2020**, *173*, 115557.
[23] D. L. Zhao, W. S. Yeung, Q. Zhao, T. S. Chung, *J. Membr. Sci.* **2020**, *604*, 118039.
[24] B. H. Jeong, E. M. V. Hoek, Y. Yan, A. Subramani, X. Huang, G. Hurwitz, A. K. Ghosh, A. Jawor, *J. Membr. Sci.* **2007**, *294*, 1.
[25] Y. Zhao, Z. Zhang, L. Dai, H. Mao, S. Zhang, *J. Membr. Sci.* **2017**, *522*, 175.
[26] J. Yin, Z. Yang, C. Y. Tang, B. Deng, *Environ. Sci. Tech. let.* **2020**, *7*, 766.
[27] C. Gropp, S. Canossa, S. Wuttke, F. Gandara, Q. Li, L. Gagliardi, O. M. Yaghi, *ACS Cent. Sci.* **2020**, *6*, 1255.

[28] S. Kandambeth, K. Dey, R. Banerjee, *J. Am. Chem. Soc.* **2019**, *141*, 1807.
[29] Z. Wang, S. Zhang, Y. Chen, Z. Zhang, S. Ma, *Chem. Soc. Rev.* **2020**, *49*, 708.
[30] Z. Xia, Y. Zhao, S. B. Darling, *Adv. Mater. Interfaces* **2020**, *8*, 2001507.
[31] L. Xu, J. Xu, B. Shan, X. Wang, C. Gao, *J. Membr. Sci.* **2017**, *526*, 355.
[32] L. Xu, T. Yang, M. Li, J. Chang, J. Xu, *J. Membr. Sci.* **2020**, *610*, 118111.
[33] Z. Zhang, X. Shi, R. Wang, A. Xiao, Y. Wang, *Chem. Sci.* **2019**, *10*, 9077.
[34] C. Tang, Y. Kwon, J. Leckie, *J. Membr. Sci.* **2007**, *287*, 146.
[35] Z. Tan, S. Chen, X. Peng, L. Zhang, C. Gao, *Science* **2018**, *360*, 518.
[36] S. Kandambeth, A. Mallick, B. Lukose, M. V. Mane, T. Heine, R. Banerjee, *J. Am. Chem. Soc.* **2012**, *134*, 19524.
[37] X. Shi, D. Ma, F. Xu, Z. Zhang, Y. Wang, *Chem. Sci.* **2019**, *11*, 989.
[38] H. Sahabudeen, H. Qi, M. Ballabio, M. Polozij, S. Olthof, R. Shivhare, Y. Jing, S. Park, K. Liu, T. Zhang, J. Ma, B. Rellinghaus, S. Mannsfeld, T. Heine, M. Bonn, E. Canovas, Z. Zheng, U. Kaiser, R. Dong, X. Feng, *Angew. Chem., Int. Ed.* **2020**, *59*, 6028.
[39] X. Song, S. Qi, C. Y. Tang, C. Gao, *J. Membr. Sci.* **2017**, *540*, 10.
[40] Y. Wang, H. Zhang, C. Song, C. Gao, G. Zhu, *J. Membr. Sci.* **2020**, *614*, 118496.
[41] R. N. Wenzel, *Ind. Eng. Chem.* **1936**, *28*, 988.
[42] J. Yin, E. S. Kim, J. Yang, B. Deng, *J. Membr. Sci.* **2012**, *423-424*, 238.
[43] X. Wu, Y. Li, X. Cui, J. Wang, X. Cao, P. Zhang, L. Zheng, *ACS Appl. Mater. Interfaces* **2018**, *10*, 10445.
[44] X. You, K. Xiao, H. Wu, Y. Li, R. Li, J. Yuan, R. Zhang, Z. Zhang, X. Liang, J. Shen, Z. Jiang, *iScience* **2021**, *24*, 102369.
[45] S. Yuan, G. Zhang, J. Zhu, N. Mamrol, S. Liu, Z. Mai, P. Van Puyvelde, B. V. Bruggen, *J. Mater. Chem. A* **2020**, *8*, 3238.
[46] Z. Y. Ma, X. Zhang, C. Liu, S. N. Dong, J. Yang, G. P. Wu, Z. K. Xu, *Chem. Commun.* **2020**, *56*, 7249.
[47] L. Shan, J. Gu, H. Fan, S. Ji, G. Zhang, *ACS Appl. Mater. Interfaces* **2017**, *9*, 44820.

SUPPORTING INFORMATION

Additional supporting information may be found in the online version of the article at the publisher's website.

How to cite this article: G. Yang, Z. Zhang, C. Yin, X. Shi, Y. Wang, *J. Polym. Sci.* **2021**, 1. https://doi.org/10.1002/pol.20210664